THE GRAVITATIONAL WAVE SIGNAL FROM MASSIVE BLACK HOLE BINARIES AND ITS CONTRIBUTION TO THE *LISA* DATA STREAM

Alberto Sesana,[1] Francesco Haardt,[1] Piero Madau,[2] and Marta Volonteri[2]

ABSTRACT

Massive black hole binaries, with masses in the range 10^3–$10^8\ M_\odot$, are expected to be the most powerful sources of gravitational radiation at mHz frequencies, and hence are among the primary targets for the planned *Laser Interferometer Space Antenna* (*LISA*). We extend and refine our previous analysis, detailing the gravitational wave signal expected from a cosmological population of massive black hole binaries. As done in our previous paper, we follow the merger history of dark matter halos, the dynamics of the massive black holes they host, and their growth via gas accretion and binary coalescences in a ΛCDM cosmology. Stellar dynamical processes dominates the orbital evolution of black hole binaries at large separations, while gravitational wave emission takes over at small radii, causing the final coalescence of the pairs. We show that the GW signal from this population, in a 3 yr *LISA* observation, will be resolved into $\simeq$90 discrete events with S/N $\geq$ 5, among which $\simeq$35 will be observed above threshold until coalescence. These "merging events" involve relatively massive binaries, $M \sim 10^5\ M_\odot$, in the redshift range $2 \lesssim z \lesssim 6$. The remaining $\simeq$55 events come from higher redshift, less massive binaries ($M \sim 5 \times 10^3\ M_\odot$ at $z \gtrsim 6$) and, although their S/N integrated over the duration of the observation can be substantial, the final coalescence phase is at too high a frequency to be directly observable by space-based interferometeres such as *LISA*. *LISA* will be able to detect a fraction $\gtrsim$90% of all the coalescences of massive black hole binaries occurring at $z \lesssim 5$. The residual confusion noise from unresolved massive black hole binaries is expected to be at least an order of magnitude below the estimated stochastic noise.

Subject headings: black hole physics — cosmology: theory — early universe — gravitational waves — relativity

Online material: color figures

1. INTRODUCTION

Gravitational radiation, described as a tensor perturbation to the metric traveling at the speed of light, is a natural consequence of Einstein's general relativity. It has been recognized (e.g., Thorne 1987) that black hole binaries are among the most important sources of gravitational waves (GW), both for ground-based interferometers such as LIGO (Abramovici et al. 1992) and VIRGO (Bradeschia et al. 1990), and for the planned *Laser Interferometer Space Antenna* (*LISA*; Bender et al. 1994).

Interferometers operate as all-sky monitors, and the data streams collect the contributions from a large number of sources belonging to different cosmic populations. A precise determination of stochastic GW backgrounds from different classes of astrophysical objects is therefore crucial to interpret the data. While a GW background may provide information on the number density, redshift evolution, and mass function of the emitting population, confusion noises add to the instrumental noise limiting the possibility of detecting other class of objects. Moreover, to optimize the subtraction of resolved sources from the data stream, it is important to have a detailed description of the expected rate, duration, amplitude, and waveforms of events.

LISA will operate in the frequency range 0.01 mHz–1 Hz, where GW emission from a cosmological population of massive black hole binaries (MBHBs) is expected to be important (Haehnelt 1994). Today, massive black holes (MBHs) are ubiquitous in the nuclei of nearby galaxies (see, e.g., Magorrian et al. 1998). If MBHs were also common in the past, and if their host galaxies experience multiple mergers during their lifetime, as dictated by popular cold dark matter hierarchical cosmologies, then MBHBs will inevitably form in large numbers during cosmic history. The formation and evolution of MBHs has been investigated recently by several groups (e.g., Menou et al. 2001; Volonteri et al. 2003a, 2003b), and the expected GW signal from in-spiraling MBH binaries has been first discussed by Rajagopal & Romani (1995), and recently by Jaffe & Backer (2003), Wyithe & Loeb (2003), Sesana et al. (2004, hereafter Paper I), and Enoki et al. (2004).

In Paper I we computed the GW background from MBHBs and the number of coalescences observable by *LISA* in a 3 yr mission, adopting the scenario for the assembly and growth of MBHs proposed by Volonteri et al. (2003a, 2003b). In such a model, "seed" holes are placed within rare high-density regions (minihalos) above the cosmological Jeans and cooling mass at redshift 20. Their evolution is followed through Monte Carlo realizations of the halo merger hierarchy combined with semi-analytical descriptions of the main dynamical processes, such as dynamical friction against the dark matter background, the shrinking of MBH binaries via three-body interactions, their co-alescence driven by the emission of gravitational waves, and the recoil associated with the nonzero net linear momentum carried away by GWs in the coalescence of two unequal mass black holes (the "gravitational rocket"). Major halo mergers lead to MBH fueling and trigger quasar activity. In this paper we use the same model to provide a more detailed characterization of the GW signal from in-spiraling MBHBs. Their contribution to the *LISA* data stream is twofold: unresolved sources will give origin to confusion noise to be compared to instrumental noise and other astrophysical stochastic backgrounds (e.g., from white dwarf binaries, Farmer & Phinney 2003), while resolved in-spiraling binaries will

[1] Dipartimento di Fisica & Matematica, Università dell'Insubria, via Valleggio 11, 22100 Como, Italy.
[2] Department of Astronomy & Astrophysics, University of California, 1156 High Street, Santa Cruz, CA 95064.

probe gravity in extreme conditions (e.g., Vecchio 2004). Confusion noise and resolved sources should provide different cosmological information. The former, produced by a large number of unresolved MBHBs, will trace light MBHBs at very high redshift, placing constraints on black hole formation scenarios prior to the reionization epoch; the latter will be a formidable tool to follow the cosmic evolution of MBHs and the formation and dynamics of MBH binaries following galaxy mergers.

The plan is as follows. In § 2 we review the basics of the detection of GW from MBHBs, defining observable quantities such as the characteristic strain amplitude, signal-to-noise ratio, and source detection rate. In § 3 we briefly summarize our scenario for the cosmological evolution of galaxy halos and associated holes. In § 4 we present confusion noise levels and source number counts. Finally, in § 5 we discuss our results.

2. GRAVITATIONAL WAVE SIGNALS

2.1. *Bursts and Periodic Events*

Following Thorne (1996), an interferometer can be characterized by two different sensitivity curves, depending on the type of signal one expects to detect, i.e., a "burst" or a "periodic" GW source. A burst, a short-lived signal whose waveform can be utterly complicated, can be described in terms of a characteristic strain amplitude h_c at the observed frequency $f_c \sim 1/\Delta t_s$, where Δt_s is the duration of the signal (Thorne 1987). The spread of the power spectrum around f_c will be $\Delta f \sim f_c$. At the other extreme, a perfectly periodic source emits, for the entire duration of the observation, at a fixed frequency f. The power spectrum will be peaked at f, with a spread $\Delta f \simeq f/N$, where N is the number of wave cycles clipped into the observation. In this respect, a burst can be thought as a single complete waveform with $f = f_c$. In the case of a periodic signal, the interferometer sensitivity is increased by the fact that, across the observing interval τ, the signal is repeated $f\tau$ times.

The sensitivity to bursts (h_B) and to periodic signals (h_P) are related by

$$h_P(f) = \frac{h_B(f)}{\sqrt{f\tau}}. \tag{1}$$

In Figure 1 the two curves h_B and h_P are compared for an assumed 3 yr *LISA* observation. The curves are obtained combining the *LISA* single-arm Michelson sensitivity curve[3] with the recent analysis of the *LISA* instrumental noise below 10^{-4} Hz (Bender 2003, extended from 3×10^{-6} to 1×10^{-6} Hz with a constant slope).

Consider now a periodic signal of finite duration, with strain amplitude h. The total energy carried by the wave will be proportional to the number of wave cycles n spent at that particular frequency. The quantity to be compared with h_B is then the "characteristic" strain $h_c \equiv h\sqrt{n}$. Note that for a periodic signal at frequency f lasting for a time interval longer than the observation time τ, we have simply $n = f\tau$. Then, the signal-to-noise ratio S/N increases by the same factor one would obtain comparing h to h_P in equation (1). The former approach, i.e., comparing h_c to h_B rather than h to h_P, is more general, as it allows us to characterize the S/N not only for perfectly periodic signals ($n = f\tau$), or for bursts ($n = 1$), but also for events in which the emitted frequency shifts to increasingly larger values during the spiral-in phase of the binary system. In the latter case, $n = n(f)$ represents the number of cycles spent in a frequency
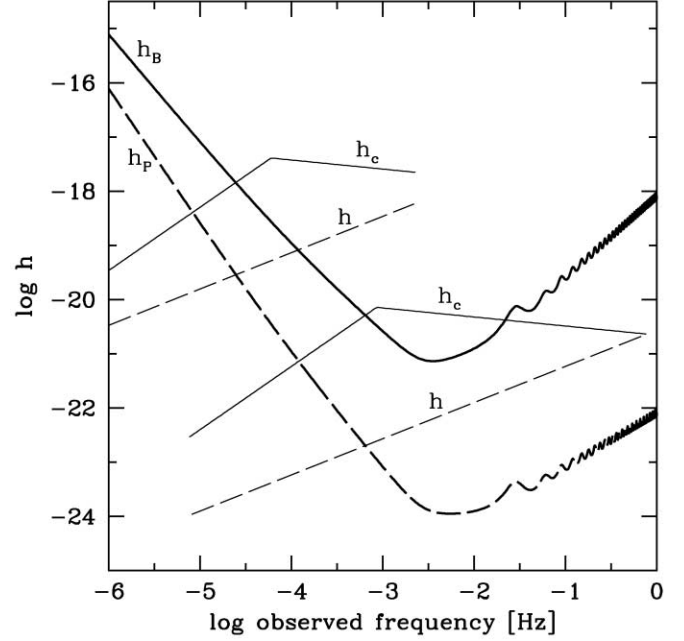
Fig. 1.—*LISA* single-arm Michelson sensitivity curve to bursts (*thick solid line*) and periodic signals (*thick dashed line*) in a 3 yr mission. Data are obtained from www.srl.clatech.edu/~shane/sensitivity and Bender (2003). The strain h (*dashed lines*) and characteristic strain h_c (*solid lines*) for a MBHB with $M_2 = 0.1M_1 = 10^5 \, M_\odot$ at $z = 1$ (*upper lines*), and $M_2 = M_1 = 10^3 \, M_\odot$ at $z = 7$ (*lower lines*) are also shown. [*See the electronic edition of the Journal for a color version of this figure.*]

interval $\Delta f \simeq f$ around frequency f, and hence h_c is the strain in a logarithmic frequency interval (Flanagan & Hughes 1998). Typically, the timescale for frequency shift is long compared to the wave period, and short compared to the duration of the observation. Only close to the innermost stable circular orbit (ISCO), the GW frequency changes at a rate comparable to the frequency itself ($n \sim 1$ and hence $h_c \sim h$). In Figure 1 we also show h and h_c for two representative binary systems. One should note that the true observable GW signal is, for $f > n/\tau$ (the "knee" frequency in the h_c curves), lower than h, as for these high frequencies the source is not monochromatic over the observation time. Such simple consideration naturally leads us to define h_c and h_B.

2.2. *Characteristic Strain*

Consider now a binary system at comoving distance $r(z)$. The strain amplitude (sky-and-polarization averaged) at the rest-frame frequency f_r is

$$h = \frac{8\pi^{2/3}}{10^{1/2}} \frac{G^{5/3} \mathcal{M}^{5/3}}{c^4 r(z)} f_r^{2/3}, \tag{2}$$

where $\mathcal{M} = (M_1 M_2)^{3/5}/(M_1 + M_2)^{1/5}$ is the "chirp mass" of the binary and all the other symbols have their standard meaning. The strain is averaged over a wave period. The rest-frame energy flux (energy per unit area per unit time) associated to the GW is

$$\frac{dE}{dAdt} = \frac{\pi}{4} \frac{c^3}{G} f_r^2 h^2. \tag{3}$$

As discussed above, the important quantity to consider is the number of cycles spent in a frequency interval $\Delta f \simeq f$ around a given frequency f. Assuming that the back-reaction from GW

emission dominates the orbital decay of a binary, during the spiral-in phase one can write

$$n \simeq f_r^2/\dot{f}_r = \frac{5}{96\pi^{8/3}}\frac{c^5}{G^{5/3}\mathcal{M}^{5/3}}f_r^{-5/3}, \qquad (4)$$

where we have used the rest-frame frequency shift rate

$$\dot{f}_r = \frac{df_r}{dt_r} = \frac{96\pi^{8/3}G^{5/3}}{5c^5}\mathcal{M}^{5/3}f_r^{11/3}. \qquad (5)$$

Note that n can be computed either in the rest or in the observer frame. The characteristic strain in an observation of (observed) duration τ is then

$$h_c = h\sqrt{n} \simeq \frac{1}{3^{1/2}\pi^{2/3}}\frac{G^{5/6}\mathcal{M}^{5/6}}{c^{3/2}r(z)}f_r^{-1/6}, \qquad n < f\tau, \quad (6)$$

and

$$h_c = h\sqrt{f\tau} \propto f_r^{7/6}, \qquad n > f\tau, \qquad (7)$$

where $f = f_r/(1+z)$ is the observed frequency. Using Parseval's theorem, it is easy to see that h_c is related to the Fourier transform of the strain $\tilde{h}$, as $h_c^2 = 2f_r^2\tilde{h}^2(f_r)$, where $\tilde{h}$ is defined over the positive frequency axis. The specific energy per unit area is then

$$\frac{dE}{dAdf_r} = \frac{\pi}{4}\frac{c^3}{G}h_c^2, \qquad (8)$$

and, from equation (6), we obtain

$$\frac{dE}{df_r} = \frac{\pi^{2/3}}{3}G^{2/3}\mathcal{M}^{5/3}f_r^{-1/3}. \qquad (9)$$

Note that $dE/df_r \propto f_r^{-1/3}$, while (eq. [3]) $dE/dt \propto f_r^{10/3}$.

2.3. Signal-to-Noise Ratio

In an operating interferometer, any stochastic signal will add up (in quadrature) to h_B to form the effective rms noise of the instrument, h_{rms}. An in-spiraling binary is then detected if the signal-to-noise ratio *integrated over the observation* is larger than the assumed threshold for detection, where the integrated S/N is given by

$$S/N_{\Delta f} = \sqrt{\int_f^{f+\Delta f} d\ln f'\left[\frac{h_c(f_r')}{h_{rms}(f')}\right]^2}. \qquad (10)$$

Here f is the (observed) frequency emitted at the starting time $t = 0$ of the observation, and Δf is the (observed) frequency shift in a time τ starting from f. The latter is implicitly given by

$$\tau = \int_f^{f+\Delta f}\frac{df'}{\dot{f}'}, \qquad (11)$$

where $df/\dot{f} = (1+z)df_r/\dot{f}_r$. The frequency at the ISCO is, strictly speaking, defined only in the test particle limit $M_2 \ll M_1$. In the general case, various estimates of the transition point from in-spiral to plunge exist, and they differ by a factor of 3 at most (e.g., Kidder et al. 1993; Cook 1994). Such uncertainties do not affect our results in any manner, so we use, for the
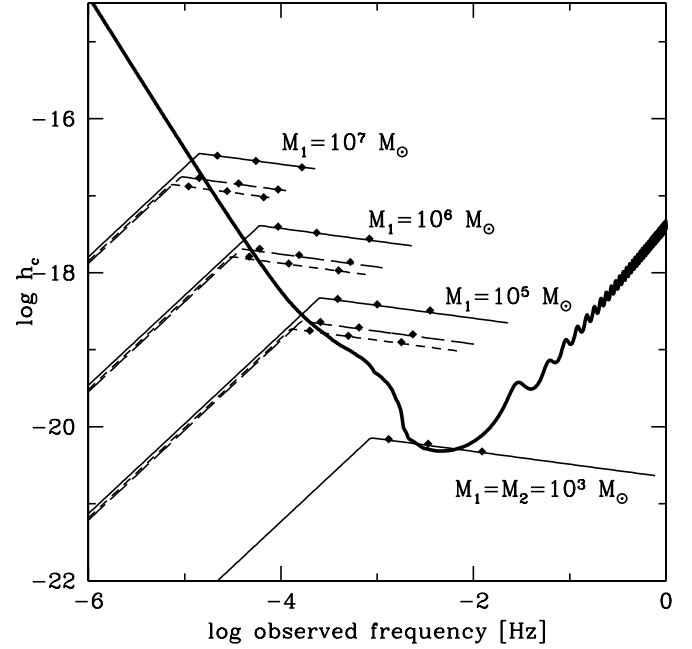

FIG. 2.—Characteristic strain h_c for MBHBs with different masses and redshifts. From top to bottom, the first three curves refer to systems with $\log(M_1/M_\odot) = 7, 6, 5$, respectively, and $M_2 = 0.1M_1$. The solid, long-dashed, and short-dashed lines assumes the binary at $z = 1, 3, 5$, respectively. A 3 yr observation is considered. The lowest solid curve assumes an equal mass binary $M_1 = M_2 = 10^3 M_\odot$ at $z = 7$. The small diamonds on each curve mark, from left to right, the observed frequency at 1 yr, 1 month, and 1 day before coalescence. The thick curve is *LISA* $5h_{rms}$ (see § 4.1), approximatively the threshold for detection with S/N ≥ 5. [*See the electronic edition of the Journal for a color version of this figure.*]

observed frequency at the ISCO, the conventional Keplerian definition:

$$f_{ISCO} = \frac{c^3}{6^{3/2}\pi G}\frac{1}{(M_1 + M_2)}(1+z)^{-1}. \qquad (12)$$

Replacing $f + \Delta f$ with f_{ISCO} in equation (11) gives τ_{ISCO}, the time needed to span the frequency interval $[f, f_{ISCO}]$, to be compared a priori to τ. In the case $\tau > \tau_{ISCO}$, we then set $f + \Delta f = f_{ISCO}$ in equation (10). In Figure 2 we plot h_c for different MBHBs at different redshifts, compared to the *LISA* h_{rms} (see § 4.1) multiplied by a factor of 5, assuming a 3 yr observation. If $h_c > 5h_{rms}$, then the signal has, approximately, an integrated S/N > 5. This is for illustrative purposes only, as the actual S/N must be integrated over the observing period using equation (10).

At frequencies higher than the "knee," the time spent around a given frequency is less than 3 yr, and $h_c \propto f^{-1/6}$. The signal shifts toward higher frequency during the observation and reaches the ISCO and the coalescence phase in most cases. The lowest curve represents a low-mass, high-redshift equal mass binary. As we shall see below, these sources are common in our hierarchical model for MBH assembly. In terms of their detectability by *LISA*, they represent a somewhat different class of events. Contrary to the case of more massive binaries present at lower z, the final coalescence phase of light binaries lies at too high frequencies, well below the *LISA* threshold.

For frequencies much below the knee, the characteristic strain is proportional to $f^{7/6}$, as the timescale for frequency shift is longer than 3 yr. The signal amplitude is then limited by the observation time, not by the intrinsic properties of the source. The source will be observed as a "stationary source," a quasi-monochromatic wave for the whole duration of the

observation. An increase in the observation time will result in a shift of the knee toward lower frequencies. The time needed for the sources to reach the ISCO starting from the knee frequency is, approximatively, the observing time. Figure 2 shows that very few stationary sources above threshold should be expected anyway.

2.4. *Coalescence Rate and Number Counts*

Given a coalescence rate R, using the frequency shift rate $\dot{f}$ (eq. [5]), we can solve for the mean number of *individual* binaries resolved during an observing period τ. We begin considering that a MBHB spans, during its lifetime, a finite frequency range, $f_{min} < f < f_{ISCO}$, where the lower limit is set to the observed frequency at the hardening radius (Quinlan 1996). Then, from continuity, the number of individual observable MBHBs can be computed as

$$N_{\tau} = R \int_{f_{min}}^{f_{ISCO}} \frac{df}{\dot{f}} + R\tau. \tag{13}$$

The first term is simply the integrated density of sources in the frequency domain, and it does not depend on τ. It is the number of sources caught in a snapshot of the entire sky. The second term is the number of new binaries born (at frequency f_{min}) during the observation time τ, and must be equal to the number of coalescences within the same period.

The general argument above does not consider that real detections must be above a specified minimum S/N, where the S/N is given by equation (10). Including a threshold criterion, the number of MBHBs with S/N $> s$ in an observation of duration τ is then

$$N_{\tau}(>s) = R \int_{f_{min}}^{f_{ISCO}} \frac{df}{\dot{f}} H_s(\Delta f) + R \int_{f_{min}}^{f_{max}} \frac{df}{\dot{f}} H_s(\Delta f_{min}), \tag{14}$$

where

$$H_s(\Delta f) = \begin{cases} 1, & S/N_{\Delta f} \geq s, \\ 0, & S/N_{\Delta f} < s. \end{cases} \tag{15}$$

In the second term of equation (14), which again accounts for the new binaries formed at the hardening radius, f_{max} is the frequency reached after 3 yr starting from f_{min}, and the function $H_s(\Delta f_{min})$ is evaluated by integration of the S/N from f_{min} to f. Given the exceedingly low value of f_{min}, this second term is totally negligible for an experiment such as *LISA*.

3. HIERARCHICAL GROWTH OF MASSIVE BLACK HOLES

The theory and method outlined in the previous sections allow us to fully characterize the expected contribution of MBHBs in the spiral-in phase to the *LISA* data stream, once the coalescence rate of MBHBs is specified. In this work a hierarchical structure formation scenario for the assembly and growth of MBHs in which seed holes form far up in the dark halo "merger tree" is assumed. We use exactly the same model discussed in Volonteri et al. (2003a, 2003b) and in Paper I. Its main features are briefly summarized in this section.

We track backward the merger history of 220 parent halos with present-day masses in the range 10^{11}–10^{15} $M_{\odot}$ with a
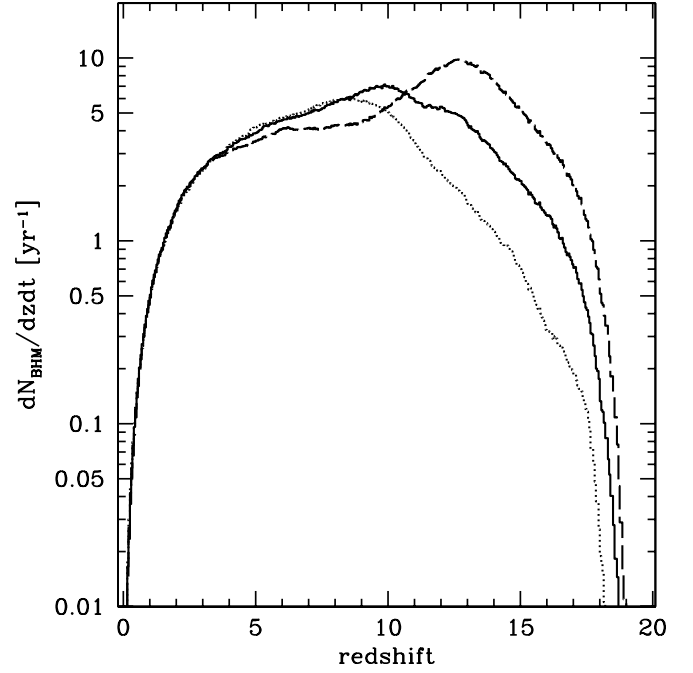

Fig. 3.—Number of coalescences of MBHBs observed per year at $z = 0$ per unit redshift. Our fiducial rate (*thick solid line*) is compared to a case in which the hardening timescale is increased by a factor of 3 (*dotted line*) or reduced by the same factor (*dashed line*). [*See the electronic edition of the Journal for a color version of this figure.*]

Monte Carlo algorithm based on the extended Press-Schechter formalism (see, e.g., Cole et al. 2000). Seed holes with $m_{seed} = 150 \, M_{\odot}$ are placed within rare high-density regions (minihalos) above the cosmological Jeans and cooling mass at redshift 20. Their evolution and growth is followed through Monte Carlo realizations of the halo merger hierarchy combined with semi-analytical descriptions of the main dynamical processes, such as dynamical friction against the dark matter background, the shrinking of MBHBs via three-body interactions, their coalescence from the emission of gravitational waves, triple MBH interactions, and the effect of gravitational recoil. Quasar activity is triggered during major mergers. We assume that the more massive hole accretes, at the Eddington rate, a gas mass fraction that scales with the fifth power of the host halo circular velocity (Ferrarese 2002).

In a typical merger event, dynamical friction drives the satellite halo toward the centre of the new forming system, leading to the formation of a bound MBHB in the violently relaxed stellar core. As the binary separation decays, the effectiveness of dynamical friction slowly declines; the bound pair then hardens by capturing stars passing within a distance of the order of the binary semimajor axis and ejecting them at much higher velocities (gravitational slingshot). The heating of the surrounding stars by a decaying MBH pair creates a low-density core out of a preexisting stellar cusp, slowing down further binary hardening (see, e.g., Milosavljevic & Merritt 2001). If the hardening continues sufficiently far, GW emission takes over, driving the pair to coalescence. Figure 3 shows the number of MBHB coalescences per unit redshift per unit observed year predicted by our model: we expect $\sim$60 coalescences per year, the vast majority involving quite light binaries ($M_1 + M_2 \leq 10^5 \, M_{\odot}$). The model was shown to reproduce rather well the observed luminosity function of optically selected quasars in the redshift range $1 < z < 5$ and the evolution of the nuclear MBH mass

density with cosmic time (Volonteri et al. 2003a) and to provide a quantitative explanation to the stellar cores observed today in bright ellipticals as a result of the cumulative eroding action of shrinking MBHBs (Volonteri et al. 2003b).

4. NUMBER COUNTS

4.1. *Stochastic Noise from MBHBs*

The customary definition of GW confusion noise level is the amplitude at which there is, on average, at least one source per frequency resolution bin. The frequency bin width is $\Delta f = 1/\tau$, so the longer the observation, the smaller the noise. As pointed out by Cornish (2003), the crude "one-bin rule" is much too simple to properly describe a binary system. Using detailed information theory, Cornish (2003) shows that a GW background becomes unresolvable when there is, on average, at least one source per eight bins.

In the last decade a considerable effort has gone into quantifying the Galactic and extragalactic confusion noise in the band 0.01 mHz–1 Hz (e.g., Schneider et al. 2001; Freitag 2001; Nelemans et al. 2001; Farmer & Phinney 2003). We have then applied the "eight-bin rule" to asses the confusion noise associated with the evolving population of MBHBs, compared to the most recent estimates of the noises from Galactic (Nelemans et al. 2001, "one-bin rule," 1 yr observation) and extragalactic (Farmer & Phinney 2003, "one-bin rule," 3 yr observation) white dwarf (WD) binaries. As shown in Figure 4, MBHBs produce confusion noise at $f \lesssim 4 \times 10^{-4}$ Hz.

Figure 4 also shows the global *LISA* $h_{\rm rms}$, along with separate contributions from different source populations. Though, as expected, MBHB stochastic noise dominates over WD-WD signals at low frequencies, it lies more than an order of magnitude below the instrumental *LISA* sensitivity curve, and hence its
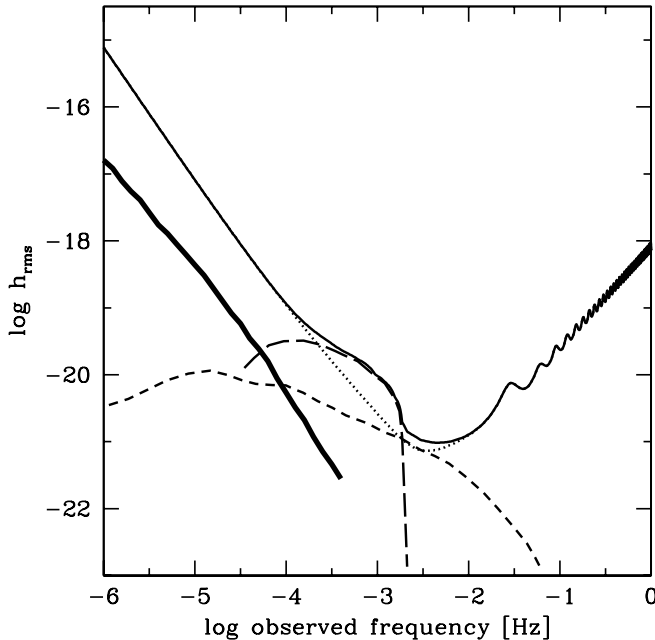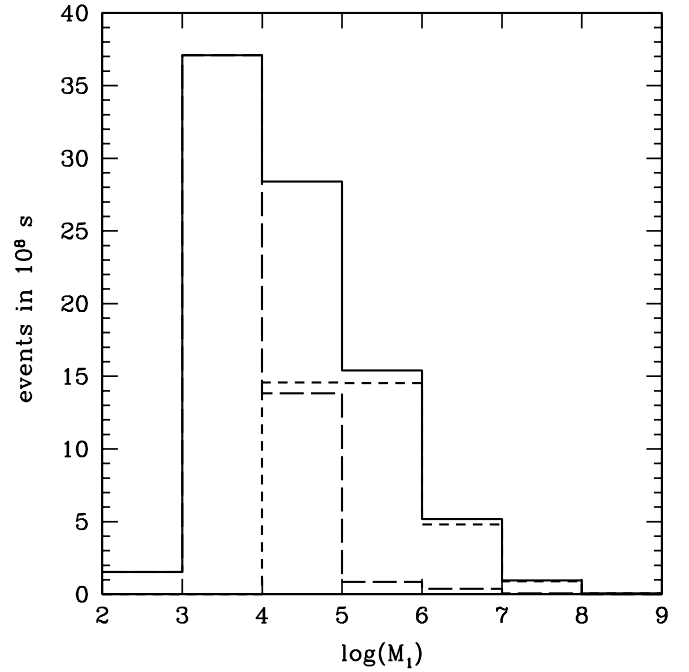

FIG. 5.—Mass distribution of the more massive member of MBHBs resolved with S/N > 5 by *LISA* in a 3 yr mission (*solid line*). The separate counts for MBs (*short-dashed line*) and IBs (*long-dashed line*) are also shown. [*See the electronic edition of the Journal for a color version of this figure.*]

contribution to the *LISA* $h_{\rm rms}$ can be ignored. On the other hand, this hampers the possibility that *LISA* could take advantage of the MBHB noise to probe the cosmological evolution of such particular parent population.

4.2. *Mass Function and Redshift Distribution*

We have divided the resolved sources into "merging" and "in-spiral" binaries (MBs and IBs, respectively). The former are those binaries that reach the ISCO during the duration of the observation with a signal above threshold. These events are of particular importance, as they probe strong field effects and represent a unique chance of observing the coalescence and ringdown phases of MBHBs. Resolved IBs, instead, do not allow a direct observation of the coalescence phase. These events arise from light binaries whose final coalescence phase lies below threshold, and from binaries of all masses with $\tau_{\rm ISCO} > 3$ yr at the very start of the observation. We expect very few IBs in this last stage anyway, because binaries above threshold have typically $\tau_{\rm ISCO} < 3$ yr when the observation starts (see Fig. 2). An example of a resolved IB is represented by the lowest curve of Figure 2. MBHBs in this class have an integrated S/N above threshold, though the coalescence phase occur at too high a frequency to be directly observed by *LISA*.

An obvious consequence of our classification is that MBs have larger mass and a lower redshift than IBs. The mass distribution of the most massive member of the binary M_1 is shown in Figure 5. The differential and cumulative redshift distributions are plotted in Figures 6 and 7, respectively. Detectable IBs are ~55 in total and account for almost all of the MBHBs observed at $z \gtrsim 7$. Conversely, the rarer MBs ($\simeq$33 in total) are confined to the redshift interval $2 \lesssim z \lesssim 7$. Figure 8 shows the average mass ratio M_2/M_1 for MBs and IBs. As expected, this is larger for IBs, given their larger average redshift. The ratio decreases at low redshift, as a consequence of the complicated
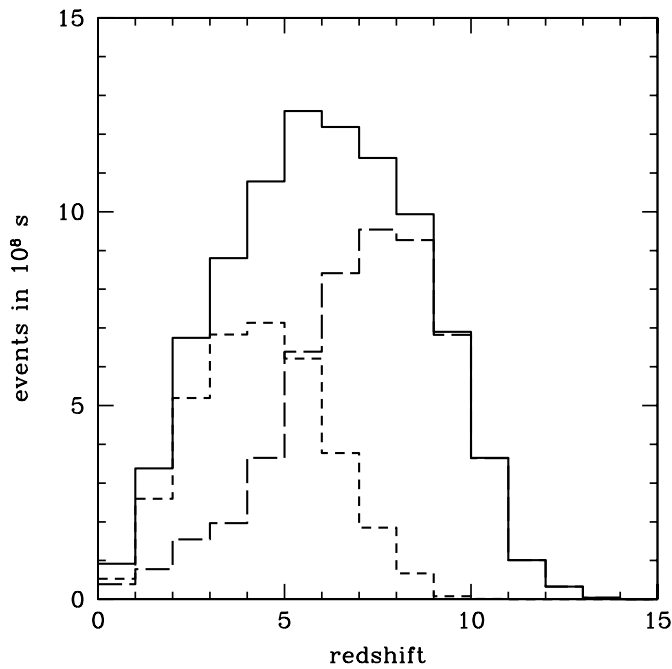

FIG. 4.—Estimated *LISA* rms confusion noise (*solid line*), as the quadratic sum of the *LISA* instrumental single-arm Michelson noise h_B (*dotted line*), the confusion noise from unresolved Galactic (Nelemans et al. 2001, *long-dashed line*) and extragalactic (Farmer & Phinney 2003, *short-dashed line*) WD-WD binaries, and our estimate of the confusion noise from unresolved MBHBs (*thick solid line*). [*See the electronic edition of the Journal for a color version of this figure.*]

Fig. 6.—Differential redshift distribution of MBHBs resolved with S/N > 5 by *LISA* in a 3 yr mission. Line style as in Fig. 5. [*See the electronic edition of the Journal for a color version of this figure.*]

Fig. 8.—Mass ratio distribution of MBHBs resolved with S/N > 5 by *LISA* in a 3 yr mission. Line style as in Fig. 5. [*See the electronic edition of the Journal for a color version of this figure.*]

merger history of host dark matter halos. The reason why the average mass ratio of MBs peaks at $M_2/M_1 \simeq 0.15$ lies in the fact that both the probability of halo mergers (because of the steep P&S halo mass function) and the dynamical friction timescale increase with decreasing halo mass ratio. Hence, fast equal mass mergers are rare, while in more common unequal mass mergers it takes longer than an Hubble time to drag the satellite hole to the centre.

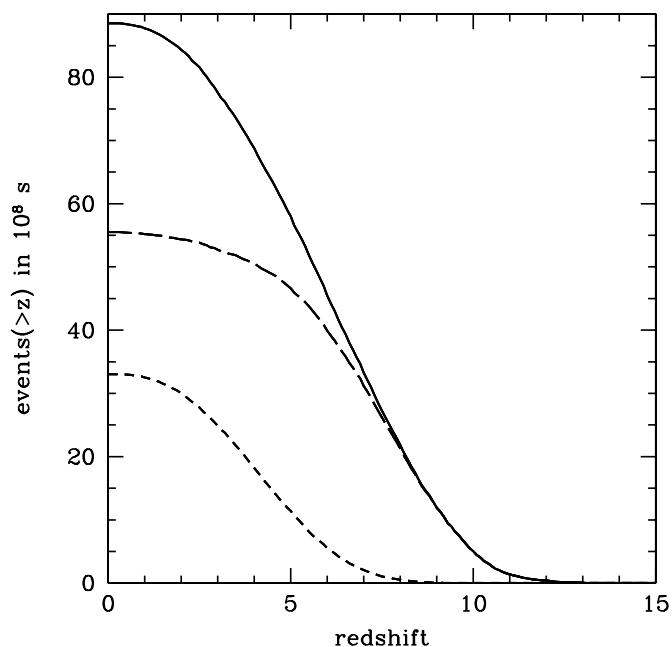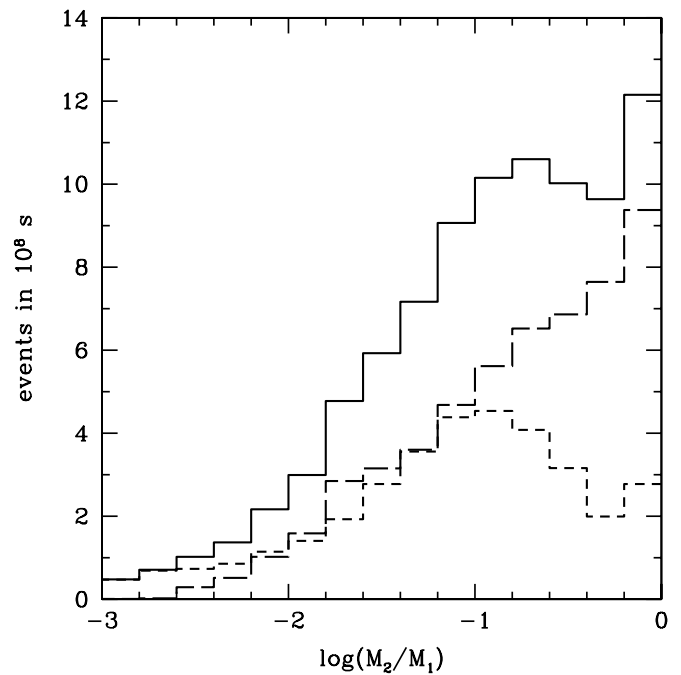We can define the detection efficiency of a specific mission as the number of observable events divided by the expected number of coalescences in the same time interval. Figure 9 shows the global (MBs+IBs) detection efficiency for *LISA* and the efficiency considering as "detections" only MBs. The large GW-brightness of MBHBs is such that *LISA* will observe ≳90% of all coalescences occurring at $z \lesssim 5$. The efficiency falls below 0.5 only for MBHBs at $z \gtrsim 8$. The efficiency to MBs only is, obviously, lower. Figure 9 shows that a space-based interferometer such as *LISA* can directly observe the final stage of
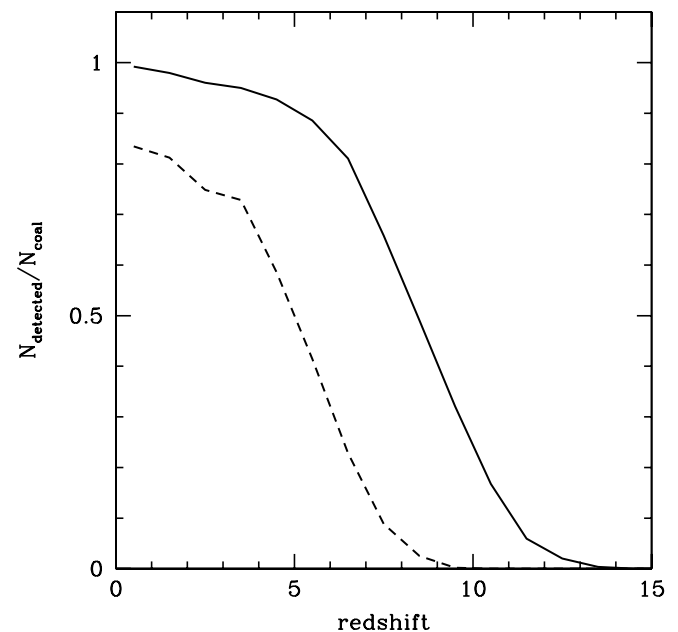

Fig. 7.—Cumulative (integral from *z* to ∞) redshift distribution of MBHBs resolved with S/N > 5 by *LISA* in a 3 yr mission. Line style as in Fig. 5. [*See the electronic edition of the Journal for a color version of this figure.*]

Fig. 9.—Detection efficiency (*solid line*), defined as the number of detected events (MBs+IBs) divided by the total number of coalescences in the same time interval, as a function of redshift. The efficiency considering only MBs as detections is also shown (*dashed line*). [*See the electronic edition of the Journal for a color version of this figure.*]

the spiral-in phase of about half of all MBHBs coalescing at $z \simeq 5$.

5. DISCUSSION

In this paper we have characterized the GW signal produced by cosmological MBHBs, and we have then folded the signal into the *LISA* performance capabilities. We find that *LISA* should resolve more than 90% of all cosmological coalescences of MBHBs occurring at $z \lesssim 5$. The detection efficiency is already $\gtrsim 0.5$ for MBHBs at $z \simeq 8$. We showed that the confusion noise from residual unresolved MBHBs is expected to be at least an order of magnitude below *LISA* instrumental noise.

We have divided the resolved events into merging and inspiral binaries. MBs are associated with systems at relatively low redshift involving heavy pairs (10^4–$10^7\ M_\odot$). Their strong GW signal can be used to study the orbital evolution of the pair until the ISCO, allowing us to test GR in extreme conditions. On the contrary, IBs are less massive pairs at higher redshift. Such systems can be generally observed, with moderate integrated S/N, only for a relatively short amount of time, from few weeks to few months, before the ISCO is reached. IBs are nevertheless important as they push the limit of observable MBHBs out to $z \simeq 12$ and allow studies of the formation and assembly of seed holes of intermediate masses. Binaries at even earlier epochs, while common in our model, are unfortunately too light to be observed by *LISA* with a relevant S/N.

In our refined study, the ~ 20 "stationary sources" discussed in Paper I, i.e., sources whose shift in frequencies Δf during the observing period is $\lesssim f$, appear to be undetectable. This is because a too optimistic sensitivity threshold for *LISA* was assumed in Paper I for frequencies below 0.1 mHz, where most of the stationary sources are expected. Indeed, an order-of-magnitude improvement of the *LISA* sensitivity below 0.1 mHz would lead to the detection of ~ 100 of such events. We stress here that our results may be sensitive to different model parameters and assumptions. As done in Paper I, we explore such possibility by running test models in which the hardening timescale t_h was divided and multiplied by a factor of 3. The resulting coalescence rates are plotted in Figure 3. We find 50 coalescences per observed year in the "slow hardening case" and 78 in the "fast hardening" case, compared to 64 in our reference model. In terms of *LISA* number counts, the effects are small. In the slow hardening case, the coalescence rate decreases at $z \gtrsim 9$ as a large fraction of binaries has t_h longer than the then Hubble time t_H. At lower redshifts it is $t_h < t_H$ anyway, the coalescence rate is basically unaffected with respect to the fiducial case, and so are the number counts (both for MBs and IBs). To obtain a significative reduction of observable sources, t_h must increase by a larger factor, so that also MBHBs in the range $5 \lesssim z \lesssim 10$ will have $t_h \gtrsim t_H$. By increasing t_h by an order of magnitude, we find the number of coalescences per observed year decreasing to 30: in a 3 yr observation *LISA* would detect 20 (40) MBs (IBs). Note that, as increasing t_h results in a lower average redshift of coalescences, this also increases the global detection efficiency. In other words, there are less sources, but a larger fraction of them is detectable.

In the fast hardening case, more binaries can coalesce at early times, and the number of surviving MBHBs at $6 \lesssim z \lesssim 12$ decreases. This ultimately causes a slight reduction in the number of IBs observable by *LISA* (49 in 3 yr, compared to 55). From Figure 3, it is also evident that, for $z \lesssim 5$, the coalescence rate is almost identical to the standard case, implying that the number of detectable MBs will remain approximately the same.

In Figure 8, we showed that IBs have an average mass ratio higher than MBs. To check whether this result depends on our assumption of equal-mass seed holes, we ran a test model with a flat initial mass function for the seed, $10\ M_\odot < m_{seed} < 500\ M_\odot$. The resulting binary mass distribution relevant for *LISA* was basically unaffected.

The vast majority of IBs are low-mass systems at fairly high redshift. Their characteristic strain lies just above the *LISA* threshold at frequencies of the order of 10^{-3}–10^{-2} Hz (see Fig. 2), where confusion noises from unresolved Galactic and extragalactic WD-WD binaries dominate the sensitivity curve (see Fig. 4). WD-WD confusion noise levels are difficult to compute because of the many uncertainties in stellar population synthesis models, and in estimating the fraction of binary stars in galaxies. In our fiducial sensitivity curve we have added to the *LISA* effective noise the Galactic WD-WD confusion noise computed by Nelemans et al. (2001), and the extragalactic WD-WD confusion noise estimated by Farmer & Phinney (2003). Note that Nelemans et al. (2001) assumed 1 yr, rather than 3 yr, integration, and both estimates employ the one-bin rule. Using the eight-bin rule we expect these noises to increase to some extent, but differences should be small. An alternative accurate estimation for Galactic WD-WD confusion noise was performed by Hils & Bender (2000), who assumed a three-bin rule. Using their noise level, which is somewhat higher than that computed by Nelemans et al. (2001), the number of IBs observed by *LISA* in 3 yr slightly decreases, from 55 to 50.

Compared to unresolved Galactic WD-WD binaries, the uncertainties in the extragalactic WD-WD confusion noise are much larger and may have a more relevant impact on number counts. The estimate of Schneider et al. (2001) lies nearly a factor of 4 above the Farmer & Phinney "fiducial" model, and this leads to a significant reduction of observable IBs, from 55 to 44. The lowest estimate we could find in the literature was the Farmer & Phinney "pessimistic" model, which is about a factor of 4 lower than their fiducial one; in this case we count 63 observable IBs.

Another potential source of noise in the frequency range 1–10 mHz is captures of compact objects (white dwarfs, neutron stars, and stellar-mass black holes) by MBHs in galaxy centers. Capture rates are quite uncertain, and estimates of relevant confusion noises span more than an order of magnitude in h_c (see Barack & Cutler 2004 for a detailed discussion). We have estimated the impact of compact object captures on *LISA* number counts assuming the more optimistic rates calculated by Freitag (2001). The number of observable IBs decreases in this case to 43. More conservative rate estimates do not affect the counts appreciably.

To summarize, in the context of our model, we can assign an approximate error of $\simeq 50\%$ to the number of high-z MBHBs detectable by *LISA*. We conclude remarking that the bulk of detections involves binaries with masses in the interval 10^3–$10^5\ M_\odot$, a range where black holes have never been observed. Genuine supermassive BH binaries, whose existence is more secure on observational grounds, appear too "heavy" for interferometers working in the band 0.01 mHz–1 Hz.

REFERENCES

Abramovici, A., et al. 1992, Science, 256, 325
Barack, L., & Cutler, C. 2004, preprint (gr-qc/0409010)
Bender, P. 2003, Classical Quantum Gravity, 20, 301
Bender, P., et al. 1994, *LISA, Laser Interferometer Space Antenna* for Gravi-
   tational Wave Measurements: ESA Assessment Study Report (Noordwijk:
   ESA)
Bradeschia, C., et al. 1990, Nucl. Instrum. Methods Phys. Res., 289, 518
Cole, L., Lacey, C. G., Baugh, C. M., & Frenk, C. S. 2000, MNRAS, 319, 168
Cook, G. B. 1994, Phys. Rev. D, 50, 5025
Cornish, N. J. 2003, preprint (gr-qc/0304020)
Enoki, M., Inoue, K. T., Nagashima, M., & Sugiyama, N. 2004, ApJ, 615, 19
Farmer, A. J., & Phinney, E. S. 2003, MNRAS, 346, 1197
Ferrarese, L. 2002, ApJ, 578, 90
Flanagan, E. E., & Hughes, S. A. 1998, Phys. Rev. D, 57, 4566
Freitag, M. 2001, Classical Quantum Gravity, 18, 4033
Haehnelt, M. G. 1994, MNRAS, 269, 199
Hils, D., & Bender, P. 2000, ApJ, 537, 334
Jaffe, A. H., & Backer, D. C. 2003, ApJ, 583, 616

Kidder, L. E., Will, C. M., & Wiseman, A. G. 1993, Phys. Rev. D, 47, 3281
Magorrian, J., et al. 1998, AJ, 115, 2285
Menou, K., Haiman, Z., & Narayanan, V. K. 2001, ApJ, 558, 535
Milosavljevic, & M., Merritt, D. 2001, ApJ, 563, 34
Nelemans, G., Yungelson, L. R., & Portegies Zwart, S. F. 2001, A&A, 375, 890
Quinlan, G. D. 1996, NewA, 1, 35
Rajagopal, M., & Romani, R. W. 1995, ApJ, 446, 543
Schneider, R., Ferrari, V., Matarrese, S., & Portegies Zwart, S. F. 2001,
   MNRAS, 324, 797
Sesana, A., Haardt, F., Madau, P., & Volonteri, M. 2004, ApJ, 611, 623 (Paper I)
Thorne, K. S. 1987, in 300 Years of Gravitation, ed. S. Hawking & W. Israel
   (Cambridge: Cambridge Univ. Press), 330
———. 1996, in IAU Symp. 165, Compact Stars in Binaries, ed. J. van
   Paradijs et al. (Dordrecht: Kluwers), 153
Vecchio, A. 2004, Phys. Rev. D, 70, 042001
Volonteri, M., Haardt, F., & Madau, P. 2003a, ApJ, 582, 559
Volonteri, M., Madau, P., & Haardt, F. 2003b, ApJ, 593, 661
Wyithe, J. S. B., & Loeb, A. 2003, ApJ, 590, 691